Soft Matter

Accepted Manuscript

ROYAL SOCIETY OF CHEMISTRY

www.rsc.org/softmatter

Soft Matter

ARTICLE

Dissipative Particle Dynamics Simulation Study on Self-Assembly of Amphiphilic Hyperbranched Multiarm Copolymers with Different Degrees of Branching†

Received 00th January 20xx,
Accepted 00th January 20xx

DOI: 10.1039/x0xx00000x

www.rsc.org/

Haina Tan,[a] Wei Wang,[b] Chunyang Yu,*[a] Yongfeng Zhou,*[a] Zhongyuan Lu*[b] and Deyue Yan[a]

Hyperbranched multiarm copolymers (HMCs) have shown great potentials to be excellent precursors in self-assembly to form various supramolecular structures in all scales and dimensions in solution. However, theoretical studies on the self-assembly of HMCs, especially the self-assembly dynamics and mechanisms, have been greatly lagging behind the experimental progress. Herein, we investigate the effect of degree of branching (DB) on the self-assembly structures of HMCs by dissipative particle dynamics (DPD) simulation. Our simulation results demonstrate that the self-assembly morphologies of HMCs can be changed from spherical micelles, wormlike micelles, to vesicles with the increase of DB, which are qualitatively consistent with the experimental observations. In addition, both the self-assembly mechanisms and the dynamic processes for the formation of these three aggregates have been systematically disclosed through the simulations. These self-assembly details are difficult to be shown by experiments and are very useful to fully understand the self-assembly behaviors of HMCs.

Introduction

In recent decades, molecular self-assembly has become a hot and promising field of research to prepare elaborate and interesting supramolecular structures,[1] such as micelles,[2] helices,[3] fibers,[4] films,[5] ribbons,[6] tubules,[7] vesicles,[8] and so on. These self-assemblies have provided great potential for applications in areas of coatings, microreactors, sensor devices, tissue engineering, drug delivery systems, and so on.[9] Among them, linear block copolymers, which consist of two or more different linear polymer blocks connected by covalent linkages, have been widely studied. They are well known as diblock copolymers, triblock copolymers, and multiblock copolymers. The influencing factors on the self-assembly of linear block copolymers include hydrophilic fraction, molecular weight, copolymer composition, polymer concentration, solvent, and external stimuli such as temperature, light, ions, or pH change.[10] Besides the great progress in experiments, computer simulations have also been used to provide detailed information on the self-assembly processes as well as self-assembly mechanisms.[11]

Dissipative particle dynamics (DPD), which is a continuum simulation technique in three dimensions and has its own advantages of fast computational speed, large integration time step, and covering much longer time scales, has been proven to be useful approach to simulate complex soft matter systems.[12-18] For example, Dormidontova and coworkers applied DPD to study the micellization kinetics and equilibrium properties of micelle solutions self-assembled from diblock copolymer.[13a] Panagiotopoulos and coworkers systematically investigated the effects of polymer composition, film thickness, and surface interact ions on the self-assembly of cylinder forming diblock copolymers confined in ultrathin films by employing DPD.[14b] Sheng and Tsao *et al*. used DPD to explore the self-assembly behaviors of coil-rod-coil triblock copolymers, including the morphological phase diagram, the mechanism of membrane fusion, and the influences of the coil length and tethered block length on membrane properties.[16d] Liang and Karniadakis *et al*. reported the shape transformations of vesicles formed from amphiphilic triblock copolymers by DPD method.[17a] These theoretical studies have greatly broadened our knowledge on the self-assembly of linear block copolymers.

As a new generation of polymer architecture, hyperbranched polymers (HBPs) have a more complex molecular structure composed of linear units, dendritic units and terminal units, and these structural units are distributed randomly along the polymer backbone.[19] Due to their unique topological structure, HBPs have demonstrated great advantages of a large population of functional groups, no or low entanglement, low solution viscosity, enhanced solubility and miscibility, and specific melt viscosity behavior.

[a] School of Chemistry and Chemical Engineering, State Key Laboratory of Metal Matrix Composites, Shanghai Jiao Tong University, 800 Dongchuan Road, Shanghai 200240, P. R. China.
E-mail: yfzhou@sjtu.edu.cn; chunyangyu@sjtu.edu.cn.
[b] Institute of Theoretical Chemistry, State Key Laboratory of Supramolecular Structure and Materials, Jilin University, Changchun 130021, P. R. China.
E-mail: luzhy@jlu.edu.cn.

† Electronic Supplementary Information (ESI) available: Schemes S1, S2, and S3 showing the simulation prototypes of the hyperbranched multiarm copolymers with different degrees of branching. Videos S1, S2, and S3 showing the formation processes of one spherical micelle, one wormlike micelle, and one vesicle, respectively. See DOI: 10.1039/x0xx00000x

Consequently, benefiting from their special physical and chemical properties, HBPs have attracted more and more attention from the scientific and engineering points of view.[20] In addition, as an extension of macromolecular self-assembly, HBPs have exhibited great potential as excellent precursors in supramolecular self-assembly. Many delicate supramolecular structures at all length scales and dimensions have been prepared through direct solution self-assembly, interfacial self-assembly, and hybrid self-assembly of HBPs.[21] However, due to the great complexity of the topological structure as well as the rapid self-assembly of HBPs, it is difficult to track the self-assembly process of HBPs in experiments. Very recently, our group has found that DPD simulation is an effective tool to disclose the details in the self-assembly of micelles and vesicles from amphiphilic HBPs, especially the self-assembly mechanisms.[22] However, up to now, the computer simulation of HBP self-assembly is still at the very beginning, and has been greatly lagging behind the experimental progress.

It is well known that degree of branching (DB) is the most important intrinsic and characteristic parameters of HBPs.[19b,23] The physichemical properties of HBPs, including the rheological property, crystallization and melting behaviors, glass transition, thermal and hydrolytic degradations, optoelectronic properties, and so on, are highly dependent on DB.[24] In addition, experimental studies have also shown that DB could give rise to great influence on the self-assembly morphology. The amphiphilic hyperbranched multiarm copolymers (HMCs) with a hydrophobic hyperbranched core and many hydrophilic linear arms (Schemes S1-S3, ESI†) could self-assemble into a series of morphologies (spherical micelle, wormlike micelle, and vesicle) by regulating the DB values in the cores.[23a,25] However, due to the limitation of experimental means, the detailed dynamics as well as mechanisms about the effect of DB on the transformations of self-assembly morphologies have not been fully understood, which should have to resort to the powerful computer simulations.

In this work, we report for the first time about the influence of DB on the self-assembly process of HMCs by using the DPD approach. Both the dynamics and mechanisms of the self-assembly of HMCs with different DBs have been carefully elucidated. The simulation results are not only in good agreement with the experimental observations, but also provide more detailed information for the self-assembly of HMCs that is difficult for experiments.

Simulation method and model details

Dissipative Particle Dynamics Method

DPD is a particle-based and mesoscopic simulation technique, which is first proposed by Hoogerbrugge and Koelman in 1992,[26] and further improved by Español and Warren.[27] In this method, each bead represents a group of molecular entities. The total force $\mathbf{F}_i$ exerted on bead i by bead j consists of three parts: a conservative force $\mathbf{F}_{ij}^C$, a dissipative force $\mathbf{F}_{ij}^D$, and a random force $\mathbf{F}_{ij}^R$, each of which is pairwise additive:

$$\mathbf{F}_i = \sum_{j\neq i}(\mathbf{F}_{ij}^C + \mathbf{F}_{ij}^D + \mathbf{F}_{ij}^R) \quad (1)$$

where the sum runs over all neighboring beads within a certain cutoff radius r_c. The three forces are given by

$$\mathbf{F}_{ij}^C = \begin{cases} a_{ij}(1 - r_{ij}/r_c)\hat{\mathbf{r}}_{ij} & (r_{ij} < r_c) \\ 0 & (r_{ij} \geq r_c) \end{cases} \quad (2)$$

$$\mathbf{F}_{ij}^D = -\gamma\omega^D(r_{ij})(\hat{\mathbf{r}}_{ij}\cdot\mathbf{v}_{ij})\hat{\mathbf{r}}_{ij} \quad (3)$$

$$\mathbf{F}_{ij}^R = \sigma\omega^R(r_{ij})\xi_{ij}\Delta t^{-1/2}\hat{\mathbf{r}}_{ij} \quad (4)$$

where α_{ij}, γ, and σ determine the strength of conservative, random, and dissipative forces, respectively. r_{ij} and $\hat{\mathbf{r}}_{ij}$ denote the distance and unit vector between beads i and j, respectively. $\mathbf{v}_{ij} = \mathbf{v}_i - \mathbf{v}_j$, $\mathbf{v}_i$ and $\mathbf{v}_j$ are the velocities of beads i and j, respectively. $\omega^D(r_{ij})$ and $\omega^R(r_{ij})$ are the distance-dependent weight functions for the dissipative force and random force, respectively. ξ_{ij} is a random number with zero average and unit variance. Moreover, in order to generate a correct equilibrium Gibbs–Boltzmann distribution, the dissipative and random forces have to satisfy the following relations:

$$\omega^D(r_{ij}) = [\omega^R(r_{ij})]^2, \quad \sigma^2 = 2\gamma k_B T \quad (5)$$

where k_B is the Boltzmann constant. According to Groot and Warren, we choose a simple form of $\omega^D(r_{ij})$ and $\omega^R(r_{ij})$ as following,[12]

$$\omega^D(r_{ij}) = [\omega^R(r_{ij})]^2 = \begin{cases} (1 - r_{ij}/r_c)^2 & (r_{ij} < r_c) \\ 0 & (r_{ij} \geq r_c) \end{cases} \quad (6)$$

In the simulation, a modified version of velocity–Verlet algorithm is used to integrate the equations of motion with a time step of $\Delta t = 0.02\tau$. For simplicity, the cutoff radius r_c, the bead mass m, and the temperature k_BT are taken as the reduced units, *i.e.*, $r_c = m = k_BT = 1$, thus the time unit $\tau = r_c\sqrt{m/k_BT} = 1$. The number density ρ is set to 3. The interaction parameter α_{ij} can be mapped to Flory-Huggins parameter χ at $\rho = 3$ as $\alpha_{ij} = \alpha_{ii} + 3.27\chi_{ij}$, where $\alpha_{ii} = 25$ is for the same type of bead and to correctly describe the compressibility of water. To keep the adjacent beads connected together along the polymer, a harmonic spring force $\mathbf{F}_{ij}^S = Cr_{ij}$ ($C = 4.0$) is adopted between bonded i-th and j-th beads.[18c]

Simulation models and details

In this study, three HMCs with the same composition but different DBs in hyperbranched cores (Schemes S1-S3, ESI†) were considered as the prototypes for the DPD simulations. Due to the Galilean invariant nature of DPD method, long-range hydrodynamics interaction (HI) is inherently incorporated in the simulations, while short-range HI is neglected since it is much weaker than hydrophobic interactions and long-range HI for the self-assembly of these HMCs. Accordingly, as schematically illustrated in Fig. 1, three DPD models denoted as $A_{30}B_{18}$ have been constructed, where the hydrophobic cores are composed of 30 purple beads (A type) and the hydrophilic arms are composed of 18 green beads (B type). Here, the DB of hyperbranched cores is determined by the equation of DB = 2D/(2D + L), where D and L are the bead numbers of dendritic and linear units, respectively.[28] As shown in Fig. 1a, there are three D beads,

and twenty-two L beads in the hyperbranched core, thus DB = 2×3/(2×3 + 22) ≈ 21%. This kind of calculation method applies to the other two models as shown in Figs. 1b-1c as well. Therefore, the DBs of the three models in cores are 21%, 35%, and 50%, respectively. In addition, S type beads represent water molecules. All simulations are performed in a cubic box of $60 \times 60 \times 60 r_c^3$ with periodic boundary conditions applied in all three dimensions. The bead number density is kept at $\rho = 3$, thus there are a total of 6.48×10^5 DPD beads in a simulation. The bead concentration, which is defined by the volume fraction of the solute, is used to characterize the concentration of HMCs and is set as 6% to guarantee the dilute aqueous solution throughout the simulations. As mentioned above, there are three types of beads (A, B, and S) in our system. For the interaction between the same beads, $\alpha_{ii} = 25$ is set to reflect the correct compressibility of the dilute solution. The interaction parameter between the arms and water is set as $\alpha_{BS} = 26$.[16b,29] In experiment, it has been proved that the solubility of HBPs with a lower DB is worse than that with a higher DB.[25] In line with it, the interaction parameters between the hyperbranched core and water are set as α_{AS} = 85, 75, and 65, respectively, with the increase of DBs from 21%, 35%, to 50%.[30] Meanwhile, the corresponding interaction parameters between the hydrophobic core and hydrophilic arms are set as α_{AB} = 70, 60, and 50, respectively. These parameters reflect the fact that, in each HMC molecule, the hyperbranched core is hydrophobic and the linear arms are hydrophilic, and the core and arms are incompatible. For each simulation, we started from randomly distributed HMCs in dilute solution, and a total of 2.00×10^6 time steps were carried out to attain equilibration for each simulation. All DPD simulations were performed with HOOMD package[31] on NVIDIA GTX 780 GPU processor.

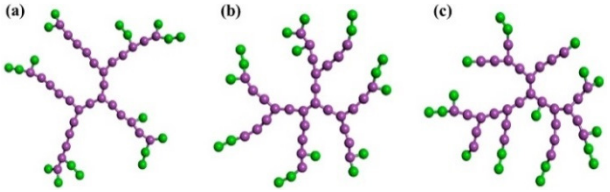

Fig. 1 Schematic structures for the three models of HMCs with different DBs in hydrophobic hyperbranched cores (purple beads, type A): (a) 21%, (b) 35%, and (c) 50%, respectively. Green beads (type B) represent hydrophilic linear arms.

Characteristic properties of simulation results

During the simulations, the radius of gyration (R_g) is calculated to characterize the size of the aggregate self-assembled from HMCs with different DBs, which is defined by

$$R_g = \sqrt{\frac{1}{N}\sum(\mathbf{r}_i - \mathbf{r}_{cm})^2}, \quad \mathbf{r}_{cm} = \frac{1}{N}\sum \mathbf{r}_i \tag{7}$$

where N is the total number of polymeric beads within the aggregate, $\mathbf{r}_i$ is the position vector of each bead, and $\mathbf{r}_{cm}$ is the center of mass of the aggregate, respectively.[32] Moreover, in order to describe the time evolution of the shape of the aggregates, we calculate three eigenvalues λ_1, λ_2, and λ_3 of the squared radius of gyration tensor.[33] First, the radius of gyration tensor of the aggregate is constructed,

$$\mathbf{A} = \begin{pmatrix} S_{xx} & S_{xy} & S_{xz} \\ S_{yx} & S_{yy} & S_{yz} \\ S_{zx} & S_{zy} & S_{zz} \end{pmatrix} \quad \text{where,} \quad \begin{matrix} S_{xx} = \frac{1}{n}\sum_{i=1}^{n}(x_i - x_{cm})(x_i - x_{cm}) \\ S_{xy} = \frac{1}{n}\sum_{i=1}^{n}(x_i - x_{cm})(y_i - x_{cm}) \end{matrix} \quad \text{etc.} \tag{8}$$

Here, n is the total number of beads in the aggregate, (x_i, y_i, z_i) is the position of the i-th bead, and (x_{cm}, y_{cm}, z_{cm}) is the coordinate of center of mass of the aggregate. After diagonalization of the matrix, we can obtain

$$\mathbf{S} = \begin{pmatrix} \lambda_1^2 & 0 & 0 \\ 0 & \lambda_2^2 & 0 \\ 0 & 0 & \lambda_3^2 \end{pmatrix} \tag{9}$$

where $\lambda_1 > \lambda_2 > \lambda_3$. Additionally, we can also use these eigenvalues to calculate the squared radius of gyration,

$$R_g^2 = \lambda_1^2 + \lambda_2^2 + \lambda_3^2 \tag{10}$$

and the asphericity,

$$\delta = \frac{(\lambda_1^2 - \lambda_2^2)^2 + (\lambda_1^2 - \lambda_3^2)^2 + (\lambda_3^2 - \lambda_2^2)^2}{2(\lambda_1^2 + \lambda_2^2 + \lambda_3^2)^2} \tag{11}$$

which indicates the shape of the aggregate and measures the deviation of the morphology away from spherical geometry.

Results and discussion

The studies of experiments have proved the close relationship between the self-assembly behaviors and the DBs of hyperbranched cores of HMCs. To address this by computer simulations, three HMC models with the same composition but different DBs of 21%, 35%, and 50% were set for the DPD simulations. The detailed self-assembly dynamics and the molecular packing structures of the aggregates will be discussed in the following sections.

DPD studies on HMCs with a DB of 21%

Fig. 2 has shown the snapshots in the self-assembly process of HMCs with a DB of 21% in dilute aqueous solutions. HMCs randomly distributed in water at the beginning (Fig. 2a). Then, these randomly distributed molecules aggregated into many small spherical micelles (Fig. 2b). Subsequently, the small spherical micelles merged with the neighboring small micelles and finally formed big spherical micelles (Figs. 2c-2e).

We also studied the real-time evolution of three eigenvalues (λ_1, λ_2, and λ_3) of the squared radius of gyration tensor of the micelles in three principal directions of the micelles. As mentioned above, one final micelle was formed through the combination of many component micelles, and in each simulation step there would be one largest component micelle. Thus, herein, the three eigenvalues of these largest component micelles at different simulation time steps were tracked continuously, and the result was shown in Fig. 2f. λ_1, λ_2, and λ_3 were almost kept equal to each other in the whole self-assembly process, which indicates the self-assemblies are almost spherical micelles at all simulation steps. Meanwhile, these three eigenvalues increased with the increase of simulation time, and then gradually levelled off. This result indicates the evolution of micelle size until the final dynamic equilibration during the self-assembly. The largest component micelles at specific simulation steps were also indicated in Fig.

2f (**I**-**IV**), which intuitively indicates the changes of micelle size and morphology during the self-assembly process.

Correspondingly, the size and the shape of the largest micelles as indicated in Fig. 2f were further quantified by the radius of gyration R_g and the asphericity δ, respectively (Table 1). The value of δ can vary from 0 to 1, where 0 and 1 correspond to a perfect spherical globule and a rod, respectively.[34] As can be seen from Table 1, the values of R_g gradually increased but the values of δ were always smaller than 0.01, which imply that the micelles are always kept spherical shape but become larger and larger with the increase of self-assembly time until to a final equilibrium.[35]

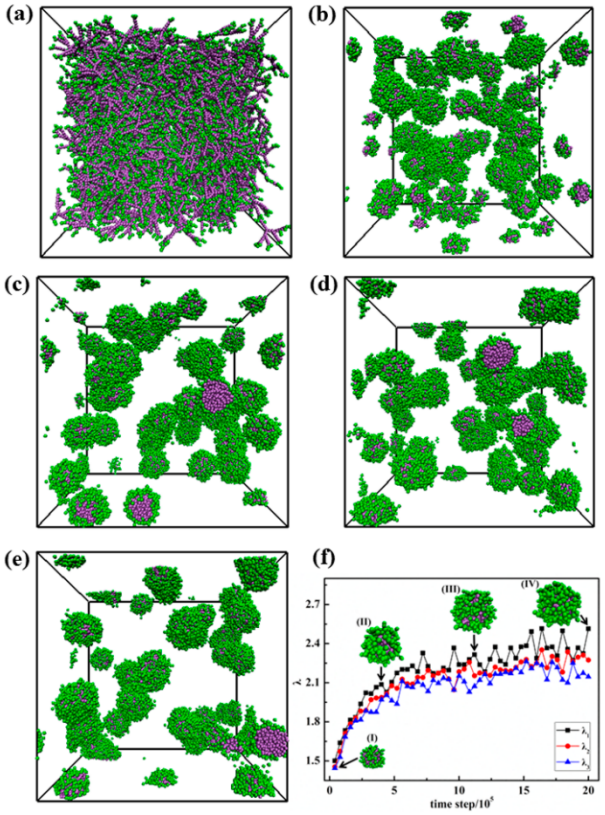

Fig. 2 Sequential snapshots of the formation of spherical micelles from HMCs with a DB of 21% at the initial state (a), 4.00 × 10^4 steps (b), 4.00 × 10^5 steps (c), 1.12 × 10^6 steps (d), and 2.00 × 10^6 steps (e). (f) The time evolution of λ_1, λ_2, and λ_3 of the largest micelles at different simulation steps. Water beads are omitted for clarity. Hydrophobic hyperbranched core is composed of purple beads, while hydrophilic linear arms are composed of green beads.

Table 1 The radius of gyration R_g and the asphericity δ of the largest micelles as indicated in Fig. 2f (**I**-**IV**)

parameters	I	II	III	IV
R_g	2.54	3.49	3.78	4.01
δ	0.0006	0.001	0.004	0.009

The evolution of micelles is driven by the fusion of micelles. To prove this, two small spherical micelles in real-time fusion evolution were taken out from the simulation snapshots to further display the pathway in detail (Fig. 3). At the beginning, the two small spherical micelles were isolated (Fig. 3a). Then they moved closer to each other and were coalesced together (Fig. 3b). Subsequently, the fusion of these two micelles proceeded with the continuous merging of the hydrophobic micelle cores (Figs. 3c-3d). Eventually, a complete spherical micelle was obtained (Fig. 3e). Moreover, in order to clearly observe the complete self-assembly process of the resulting spherical micelles, the video clip of one spherical micelle chosen from the simulation box was made and shown in the ESI† (Video S1).

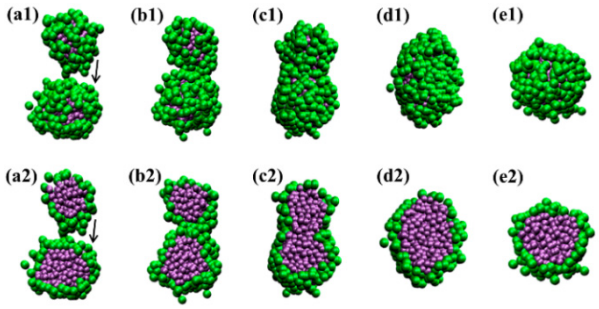

Fig. 3 Real-time fusion of two small spherical micelles into one big spherical micelle in the simulation at 3.80 × 10^5 steps (a), 3.82 × 10^5 steps (b), 3.84 × 10^5 steps (c), 3.86 × 10^5 steps (d), and 3.90 × 10^5 steps (e). For each snapshot from (a) to (e), the upper one is the whole view, while the lower one is the cross-sectional view. Water beads are omitted for clarity. The color codes are the same as those in Fig. 2.

Furthermore, the DPD simulation results can also provide more details of the self-assembly structure, which could provide valuable microscopic insights for the formation of the aggregate. Fig. 4a displays a cross-sectional view of a magnified spherical micelle chosen from Fig. 2e. Evidently, the spherical micelle is composed of an inner kernel formed by the aggregated hydrophobic hyperbranched cores, surrounded by an outer corona formed by the hydrophilic arms. To clearly display molecular packing structure of the spherical micelle, two HMCs in the cross-section were labelled with different colors, and it shows that each HMC is microphase-separated into a cone-shaped geometry with segregated core and arms. Thus, for the HMCs with a low DB, they might undergo a spherical-to-cone microphase separation to construct the spherical micelles as shown in Fig. 4b.[22a]

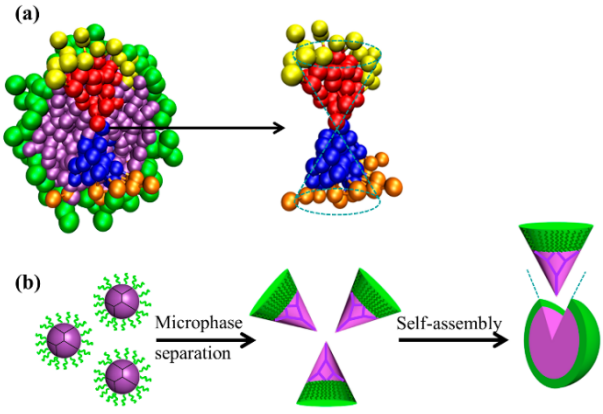

Fig. 4 The fine structure of one spherical micelle: (a) Cross-sectional view of the spherical micelle, and the arrow indicated the two labelled molecules in the cross-section. (b) The corresponding schematic representation of the microphase separation process and the molecular packing model in the spherical micelle. Hydrophobic hyperbranched core: purple, red, and blue beads; hydrophilic linear arms: green, yellow, and orange beads. Water beads are omitted for clarity.

DPD studies on HMCs with a DB of 35%

Fig. 5 has shown the self-assembly process of HMCs with a DB of 35%. At the beginning, HMCs randomly distributed in water (Fig. 5a), and then they aggregated into spherical micelles (Figs. 5b-5c). Subsequently, these spherical micelles grew into small (Fig. 5d), short (Fig. 5e), and finally long wormlike micelles (Fig. 5f).

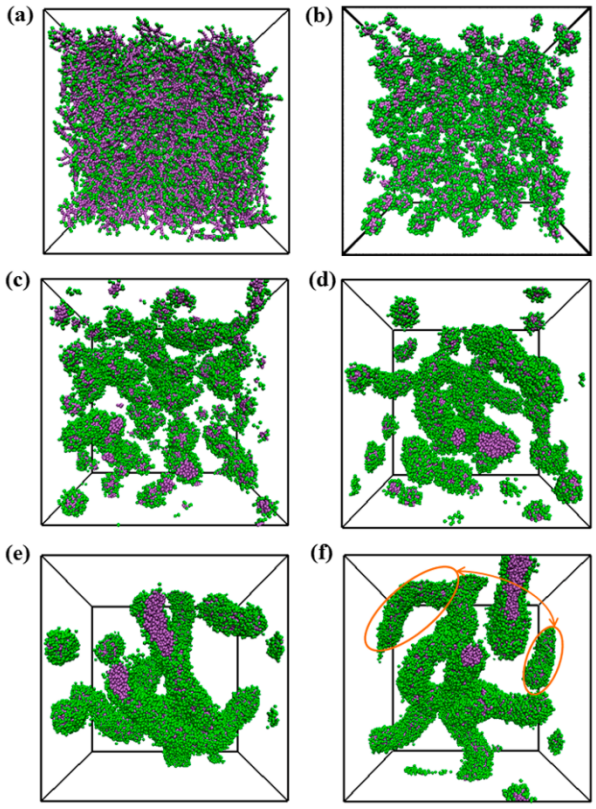

Fig. 5 Sequential snapshots of the formation of wormlike micelles from HMCs with a DB of 35% at the initial state (a), 4.00 × 10^4 steps (b), 2.80 × 10^5 steps (c), 4.80 × 10^5 steps (d), 9.60 × 10^5 steps (e), and 2.00 × 10^6 steps (f). The two wormlike micelles indicated by the two orange circles in image (f) represent one long wormlike micelle, which is separated by the periodic boundary conditions applied in all three dimensions. Water beads are omitted for clarity. The color codes are the same as those in Fig. 2.

Meanwhile, we selected a final long wormlike micelle, and further studied the real-time evolution of λ_1, λ_2, and λ_3 of the largest component micelles at sequential simulation steps in Fig. 6. There are four stages in the self-assembly process. In the first stage, these three eigenvalues were almost kept equal to each other and gradually increased with simulation time (Fig. 6, inset), indicating the formation and evolution of spherical micelle. Thus, stage **1** is featured as the formation of spherical micelle. In the second stage, λ_1 was suddenly increased into a value around 5 and then gradually kept stable, while λ_2 and λ_3 were kept nearly constant. Thus, stage **2** is featured as the formation of small wormlike micelle. In the third stage, λ_1 was jumped into a value around 7.5, while λ_2 and λ_3 was still kept nearly constant. Thus, stage **3** is featured as the formation of short wormlike micelle. In the fourth stage, λ_1 was further jumped into a value around 12 with λ_2 and λ_3 nearly constant. Thus, stage **4** is featured as the formation of long wormlike micelle. Moreover, the largest component micelles at specific simulation steps were also indicated in Fig. 6 (**I-V**), which intuitively indicates the changes of micelle size and morphology during the self-assembly.

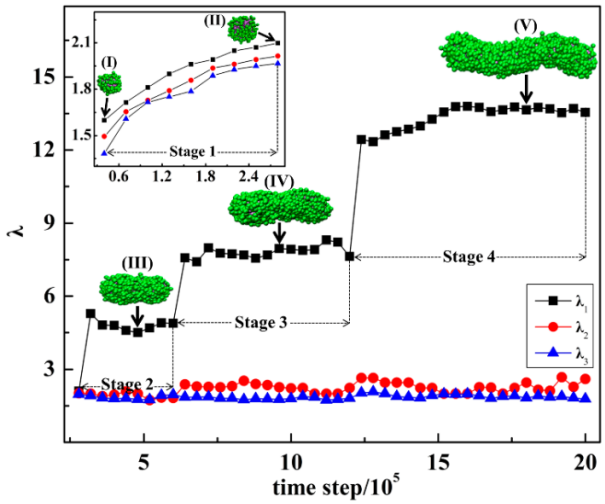

Fig. 6 The time evolution of λ_1, λ_2, and λ_3 of the largest component micelles of a final long wormlike micelle at different simulation steps. Water beads are omitted for clarity. The color codes are the same as those in Fig. 2.

Correspondingly, the size and the shape of the largest micelles as indicated in Fig. 6 were further quantified by the radius of gyration R_g and the asphericity δ, respectively (Table 2). The values of R_g increased from 2.59 to 13.98, indicating that the micelles gradually grow larger. The values of δ for **I** and **II** were close to zero, implying that the micelles are kept spherical shape at the beginning. Subsequently, the values of δ gradually increased from 0.37 to 0.86 (**III-V**), which suggests that the micelles turn into wormlike micelles.

Table 2 The radius of gyration R_g and the asphericity δ of the largest micelles as indicated in Fig. 6 (**I-V**)

parameters	I	II	III	IV	V
R_g	2.59	3.51	5.23	8.46	13.9
δ	0.007	0.001	0.37	0.69	0.86

According to Fig. 6, there are four stages in the self-assembly of long wormlike micelle, however, the detailed pathways for these self-assembly stages are still unknown. Thus, the sequential snapshots of the micelles in all these stages were captured to disclose the pathways. The first stage is similar to the process of spherical micelles self-assembled from HMCs with a DB of 21%, and thus is not shown here again. The detailed pathway for the second stage is displayed in Fig. 7. The two small spherical micelles were coalesced together, and then they were gradually laterally fused with each other to form one small wormlike micelle. The third stage involves the transition from the small wormlike micelle to the short wormlike micelle, which is induced through the lateral fusion between small spherical micelle and small wormlike micelle, as depicted in Fig. 8. The fourth stage is attributed to the formation of long wormlike micelles, which involves the end-to-end fusion of two short wormlike micelles as shown in Fig. 9. In summary, the dynamic formation process of wormlike micelles could be schematically shown in Fig. 10, and there are

three kinds of lateral fusion processes including the "sphere to sphere" fusion (Fig. 10a), "rod to sphere" fusion (Fig. 10b), and "rod to rod" fusion (Fig. 10c). To further illustrate this, a complete self-assembly process of the wormlike micelle was shown in the video in the ESI† (Video S2).

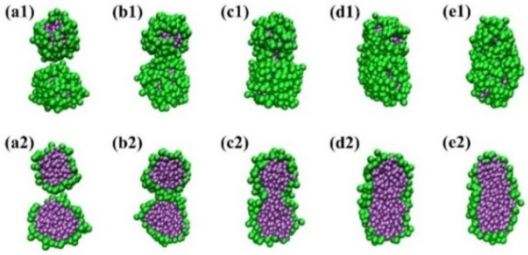

Fig. 7 A real-time lateral fusion process from two small spherical micelles into one small wormlike micelle in the simulation at 2.80 × 10^5 steps (a), 2.96 × 10^5 steps (b), 3.10 × 10^5 steps (c), 3.22 × 10^5 steps (d), and 3.36 × 10^5 steps (e). For each snapshot from (a) to (e), the upper one is the whole view, while the lower one is the cross-sectional view. Water beads are omitted for clarity. The color codes are the same as those in Fig. 2.

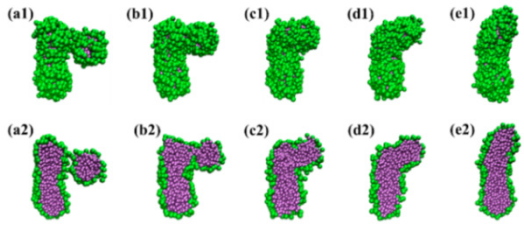

Fig. 8 A real-time fusion process between small spherical micelle and small wormlike micelle to form short wormlike micelle in the simulation at 6.02 × 10^5 steps (a), 6.12 × 10^5 steps (b), 6.26 × 10^5 steps (c), 6.38 × 10^5 steps (d), and 6.60 × 10^5 steps (e). For each snapshot from (a) to (e), the upper one is the whole view, while the lower one is the cross-sectional view. Water beads are omitted for clarity. The color codes are the same as those in Fig. 2.

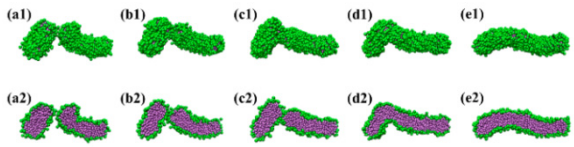

Fig. 9 A real-time end-to-end fusion process of two short wormlike micelles into one long wormlike micelle in the simulation at 1.186 × 10^6 steps (a), 1.202 × 10^6 steps (b), 1.210 × 10^6 steps (c), 1.236 × 10^6 steps (d), and 1.250 × 10^6 steps (e). For each snapshot from (a) to (e), the upper one is the whole view, while the lower one is the cross-sectional view. Water beads are omitted for clarity. The color codes are the same as those in Fig. 2.

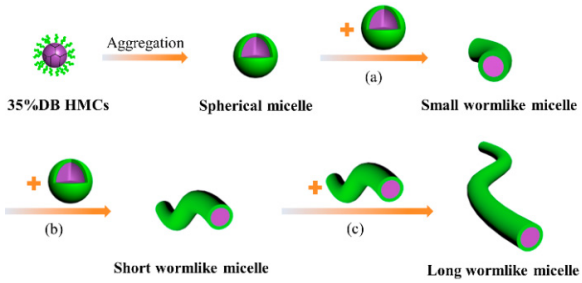

Fig. 10 Schematic representation for the dynamic formation process of wormlike micelles from HMCs with a DB of 35% in hydrophobic hyperbranched core. (a) The "sphere to sphere" lateral fusion; (b) The "rod to sphere" lateral fusion; and (c) The "rod to rod" lateral fusion.

The simulation can also provide the molecular packing model inside the wormlike micelles. According to the magnified wormlike micelle as shown in Fig. 11a, the micelle has a completely segregated kernel-shell structure. The hydrophobic cores of HMCs are packed in the micelle kernel and the hydrophilic arms are outspread in water to stabilize the micelle. In addition, two labelled HMCs in the cross-section were separated, and it shows that each HMC is microphase-separated into a truncated cone-shaped geometry with segregated core and arms. Thus, for the HMCs with a DB of 35%, they might undergo a spherical-to-truncated cone microphase separation to construct the wormlike micelles as shown in Fig. 11b.

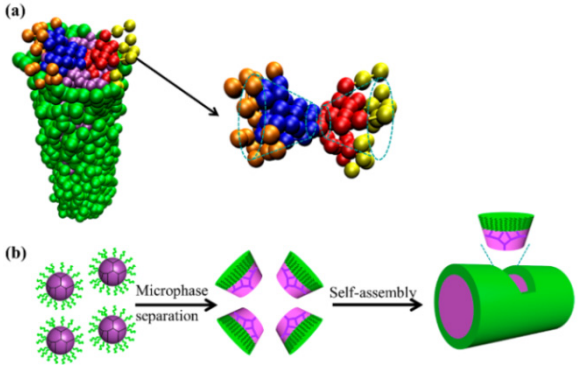

Fig. 11 The fine structure of one wormlike micelle: (a) A magnified view of the wormlike micelle, and the arrow indicated two labelled molecules on the cross-section of the wormlike micelle. (b) The corresponding schematic representation of the microphase separation process and the molecular packing model in the wormlike micelle. Hydrophobic hyperbranched core: purple, red, and blue beads; hydrophilic linear arms: green, yellow, and orange beads. Water beads are omitted for clarity.

DPD studies on HMCs with a DB of 50%

Fig. 12 has shown the self-assembly process of HMCs with a DB of 50%. At the beginning, HMCs randomly distributed in water (Fig. 12a). Then, these randomly distributed HMCs aggregated into spherical micelles (Fig. 12b). And then, the spherical micelles transformed into wormlike micelles (Fig. 12c). Subsequently, the wormlike micelles transformed into membranes (Fig. 12d). Finally, the flexible membranes bended (Fig. 12e), and closed to form vesicles (Fig. 12f).

The three eigenvalues λ_1, λ_2, and λ_3 of the largest component aggregates in each simulation step of a final vesicle were calculated, as shown in Fig. 13a. The change trend of these eigenvalues is more complex than that of the previous two HMC systems, and there are about six stages can be discerned in the self-assembly process. As depicted in the inset of Fig. 13a, at the beginning, λ_1, λ_2, and λ_3 were almost equal to each other below 1.20 × 10^4 simulation steps, indicating the formation of spherical micelles. So it is a stage (stage **1**) featured as the formation of spherical micelles, which is also proved by the direct morphology observation from aggregate **I** (Fig. 13b). Then, λ_1 went on increasing from 2.0 to 6.2, while λ_2 and λ_3 were kept nearly constant, indicating the formation of anisotropic supramolecular structures. The direct morphology observation of aggregate **II** (Fig. 13b) indicates that they are wormlike micelles. Thus, the stage **2** is featured as the transformation from spherical micelles into wormlike micelles. In stage **3**, λ_2 started to increase from 1.7 to 6.0, while λ_3 was still kept nearly constant. The morphology observations indicate that the wormlike micelles (aggregate **II**) gradually

fuse with each other (aggregate **III**) to form membrane (aggregate **IV**) in this stage. Thus, the stage **3** is featured as the transformation from wormlike micelles to membrane. In stage **4**, both λ_2 and λ_3 just changed a bit, and only an undulation of membrane was observed from aggregate **IV** to aggregate **V**. Subsequently, in stage **5**, λ_3 jumped from 2 to 4.5, while λ_2 was almost kept constant. It is a stage for the bending (aggregate **VI**) and closing (aggregate **VII**) of the membrane to form vesicle (aggregate **VIII**). Finally, in stage **6**, the three eigenvalues were kept equal to each other again, and it is a stage attributed to the undulation of spherical vesicle (aggregate **IX**). It should be noted that the changes of λ_1 became very complex after 4.0×10^4 simulation steps, so only λ_2 and λ_3 were used to determine the self-assembly processes from stages **3** to **6**.

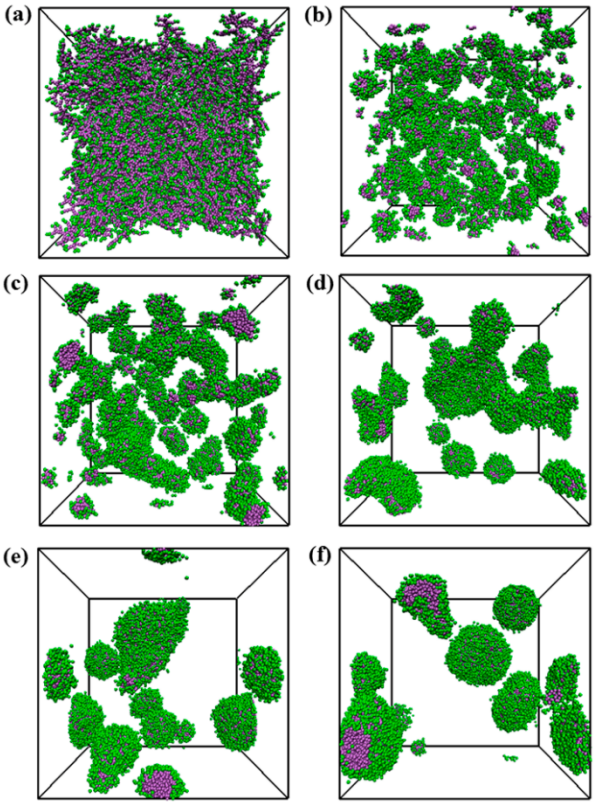

Fig. 12 Sequential snapshots of the formation of vesicles from HMCs with a DB of 50% at the initial state (a), 8.00×10^3 steps (b), 4.00×10^4 steps (c), 7.20×10^5 steps (d), 8.80×10^5 steps (e), and 2.00×10^6 steps (f). Water beads are omitted for clarity. The color codes are the same as those in Fig. 2.

Correspondingly, the size and the shape of the largest aggregates as shown in Fig. 13b were further quantified by R_g and δ, respectively (Table 3). The values of Rg for aggregates **I** to **III** increased from 3.18 to 10.01, indicating that the aggregates gradually grow larger, while the values of δ were 0.009, 0.67, and 0.34, respectively, indicating that the morphologies of the aggregates go through from sphere, wormlike, to membrane-like structure. Both R_g and δ for aggregates **III** to **IV** decreased, implying the formation of complete membrane. The values of R_g and δ for aggregates **IV** and **V** were almost equal, indicating the undulation of the membrane. The values of R_g from aggregates **V** to **IX** decreased from 9.20 to 8.46, while the values of δ decreased from 0.20 to 0.006, implying that the membrane was gradually bent and then closed to vesicle.

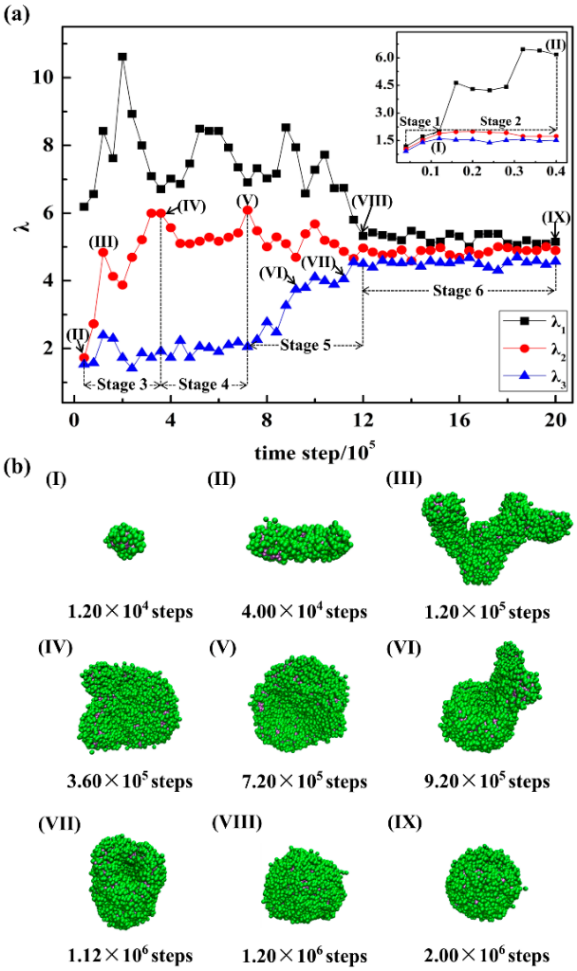

Fig. 13 (a) The time evolution of λ_1, λ_2, and λ_3 of the largest aggregates of a final vesicle at different simulation steps. (b) The corresponding morphologies of the largest aggregates (**I-IX**). Water beads are omitted for clarity. The color codes are the same as those in Fig. 2.

Table 3 The radius of gyration R_g and the asphericity δ of the largest aggregates as indicated in Fig. 13b (**I-IX**)

parameters	I	II	III	IV	V
	VI	VII	VIII	IX	
R_g	3.18	6.60	10.01	9.20	9.20
	9.11	8.72	8.56	8.46	
δ	0.009	0.67	0.34	0.20	0.20
	0.09	0.027	0.009	0.006	

During the formation of vesicle, the first two stages are similar to the process of short wormlike micelles self-assembled from HMCs with a DB of 35%; however, the detailed pathways for the formation of membrane and vesicle are still unknown. Thus, the sequential snapshots of the aggregates were captured to disclose the pathways. As can be seen from Fig. 14, the very short wormlike micelle could laterally fuse with the neighboring micelle to form small membrane (Figs. 14a-14c), and then the small membrane

gradually laterally fused with the neighboring wormlike micelle to form large membrane (Figs. 14d-14i). Subsequently, the large membrane gradually bent and curled up to form a bowl-like structure (Figs. 15a-15c). Finally, the bowl-like structure closed to form a spherical vesicle (Figs. 15d-15f). On the basis of the above results, the dynamic formation process of the vesicle could be schematically summarized as shown in Fig. 16. To further illustrate this, a complete self-assembly process of the vesicle was shown in the video in the ESI† (Video S3).

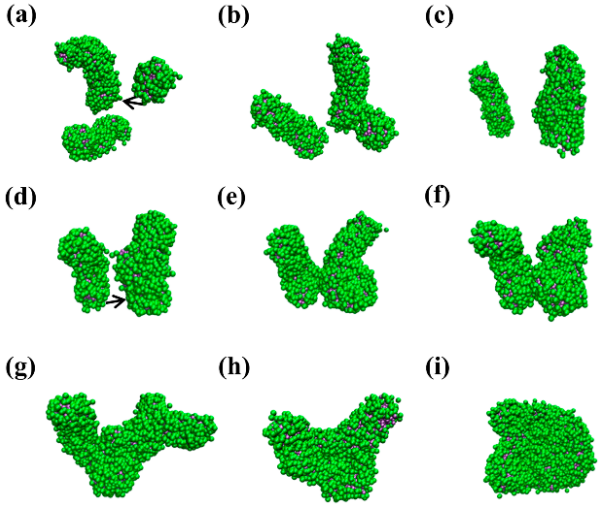

Fig. 14 A real-time growth process of membrane in the simulation at 6.80×10^4 steps (a), 7.60×10^4 steps (b), 8.40×10^4 steps (c), 9.20×10^4 steps (d), 1.00×10^5 steps (e), 1.08×10^5 steps (f), 1.20×10^5 steps (g), 2.00×10^5 steps (h), and 3.60×10^5 steps (i). Water beads are omitted for clarity. The color codes are the same as those in Fig. 2.

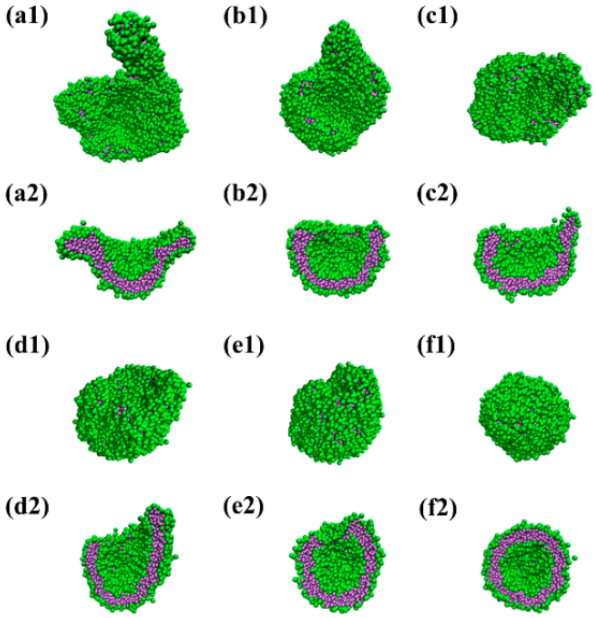

Fig. 15 A real-time self-assembly dynamics of vesicle through the bending and closing of the membrane in the simulation at 7.80×10^5 steps (a), 8.60×10^5 steps (b), 9.80×10^5 steps (c), 1.08×10^6 steps (d), 1.12×10^6 steps (e), and 1.28×10^6 steps (f). For each snapshot from (a) to (f), the upper one is the whole view, while the lower one is the cross-sectional view. Water beads are omitted for clarity. The color codes are the same as those in Fig. 2.

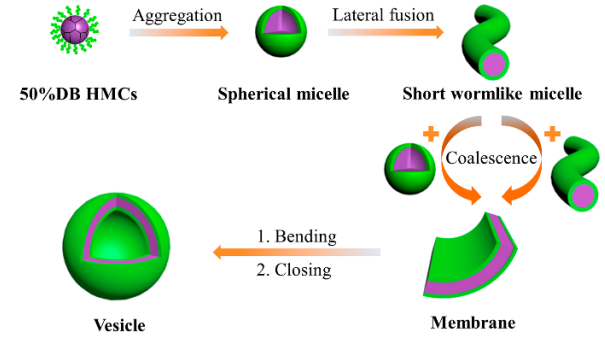

Fig. 16 Schematic representation for the dynamic formation process of vesicle from HMCs with a DB of 50% in hydrophobic hyperbranched core.

Moreover, two labelled HMCs in the cross-section were separated and magnified, and it shows that the molecular geometry of each HMC is in cylindrical shape, and the two HMCs are packed together in a head-to-tail manner to form the bilayer (Fig. 17a). Thus, for the HMCs with a DB of 50%, they might undergo a spherical-to-cylindrical microphase separation to construct the vesicles as depicted in Fig. 17b.

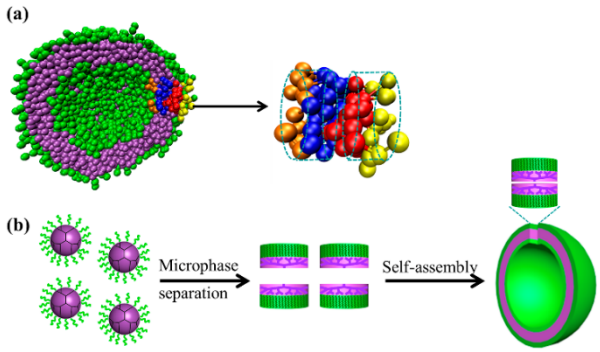

Fig. 17 The fine structure of one vesicle: (a) Cross-sectional view of the vesicle, and the arrow indicated the two labelled molecules extracted from the vesicle to show the molecular packing model. (b) The corresponding schematic representation of the microphase separation process and the molecular packing model in the vesicle. Hydrophobic hyperbranched core: purple, red, and blue beads; hydrophilic linear ar green, yellow, and orange beads. Water beads are omitted for clarity.

Discussions

The above simulation results indicate that as DB increases, the self-assembly morphologies of HMCs vary from spherical micelles, wormlike micelles, to vesicles, and the correspondi dimensions are from zero-dimension (0D), one-dimension (1D to two-dimension (2D), as displayed in Fig. 18. For the HMCs with a low DB in the cores, they first aggregated into many small spherical micelles, and then the small micelles furth fused into some big spherical micelles. In the packing model of the spherical micelle, each HMC was microphase-separated into a cone-shaped structure. For the HMCs with a middle DB in the cores, they first underwent a similar self-assembly process to that of HMCs with a low DB to form spherical micelles. Subsequently, these spherical micelles experienced three kinds of sequential lateral fusion processes to get the long wormlike micelles, including “sphere to sphere” fusion to form small wormlike micelles, “rod to sphere” fusion to fo short wormlike micelles, and “rod to rod” fusion to form long wormlike micelles. In the packing model, each HMC

experienced a spherical-to-truncated cone microphase separation to construct the wormlike micelles. For the HMCs with a high DB in the cores, they first aggregated to wormlike micelle, which is similar to the self-assembly process of HMCs with a middle DB. Then the wormlike micelles laterally fused with each other to form membranes. Finally, the membrane was gradually bent and then closed to a bilayer vesicle. In this packing model, each HMC went through a spherical-to-cylindrical microphase separation to construct the vesicles.

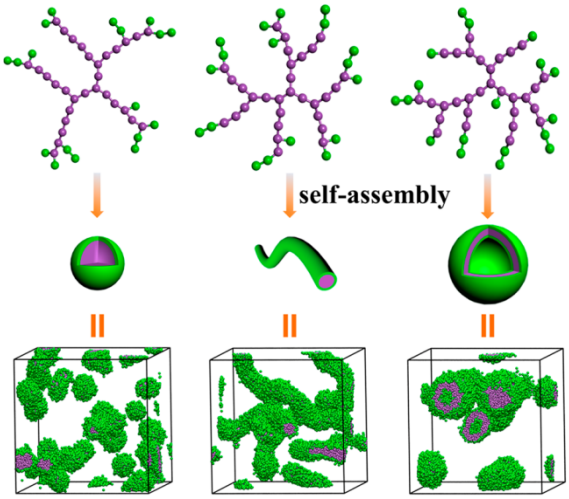

Fig. 18 DB-dependent morphology transformation in the self-assembly of HMCs with variable DBs in the hydrophobic hyperbranched cores. Water beads are omitted for clarity. The color codes are the same as those in Fig. 2.

Therefore, as the DB increases, the microphase separation of HMCs varies from cone, truncated cone, to cylinder, while the self-assembly morphology changes from spherical micelles, wormlike micelles, to vesicles. Such results verify that the theory of the packing parameter is suitable for investigating the self-assembly behaviors of HMCs.[36,37] These simulation results are consistent with the experimental findings, and the synthesized amphihilic HMCs with different DBs in the hyperbranched cores (Schemes S1-S3, ESI†) have shown the self-assembly structures changing from spherical micelles, wormlike micelles, to vesicles with the increase of DBs from 20%, 33%, to 44%.[25] Besides, the similations also provide much more details for the self-assembly process including the self-assembly dynamics and molecular packing structures in the self-assemblies, which are very hard for experiments.

The main reason for the DB-dependent self-assembly as summarized in Fig. 18 is the different hydrophobicity situated at different DBs in hyperbranched cores. It is well known that HBPs have better solubility than the corresponding linear analogues,[19b,20a,25,38] and the same is true for HMCs. In other words, the solubility of HBPs with a higher DB is better than those with a lower DB. Thereby, the repulsive interaction between the hydrophobic hyperbranched core and water declines as DB increases, and this result leads to the decrease of incompatibility between the core and the arms on the premise that the parameter between the hydrophilic arms and water is constant. The different interaction parameters caused by different DBs in HBPs determine the variation of the microphase separation behaviors, which leads to the morphology transformation of the self-assembled aggregates.

Conclusions

In summary, we have successfully applied the DPD simulation technique to study the self-assembly behaviors of hyperbranched multiarm copolymers with hydrophobic cores of different degrees of branching. The molecular packing models in the self-assembly structures, as well as the self-assembly mechanisms and the dynamics have been disclosed in detail. The results indicate that with the increase of degrees of branching from 21% to 50%, the self-assembly morphologies of hyperbranched multiarm copolymers change from spherical micelles, wormlike micelles, to vesicles, which are in excellent agreement with the experimental observations. The most important thing for the DPD simulation is that it can provide many details for the self-assembly process which are difficult to be captured by experiments. For example, the DPD simulation results indicate that the hyperbranched multiarm copolymers with a low degree of branching undergo a co microphase separation to pack into spherical micelles; the hyperbranched multiarm copolymers with a middle degree of branching undergo a truncated cone microphase separation to construct the wormlike micelles through continuous fusion steps of spherical micelles and short wormlike micelles; and the hyperbranched multiarm copolymers with a high degree of branching undergo a cylindrical microphase separation to construct the vesicles through the intermediates from spheres, wormlike micelles, membranes, to vesicles. These simulation results provide a detailed understanding on the relationship between the topological architectures of polymers and the self-assemblies.

Acknowledgements

We thank the National Basic Research Program (2013CB834506), China National Funds for Distinguished Young Scholar (21225420), National Natural Science Foundation of China (21404070, 2144062, 91127047), and "Shu Guang" project supported by Shanghai Municipal Education commission and Shanghai Education Development Foundation (13SG14) for financial support.

Notes and references

1 (a) G. M. Whitesides and B. Grzybowski, *Science*, 2002, **295**, 2418; (b) S. G. Zhang, *Nat. Biotech.*, 2003, **21**, 1171; (c) R. F. Service, *Science*, 2005, **309**, 95; (d) V. Percec, D. A. Wilson, P. Leowanawat, C. J. Wilson, A. D. Hughes, M. S. Kaucher, D. A. Hammer, D. H. Levine, A. J. Kim and F. S. Bates, *Science*, 2010, **328**, 1009.

2 (a) Y. Y. Won, H. T. Davis and F. S. Bates, *Science*, 1999, **283**, 960; (b) D. J. Pochan, Z. Y. Chen, H. G. Cui, K. Hales, K. Qi and K. L. Wooley, *Science*, 2004, **306**, 94; (c) S. Kubowicz, J. F. Baussard, J. F. Lutz, A. F. Thunemann, H. von Berlepsch and A Laschewsky, *Angew. Chem., Int. Ed.*, 2005, **44**, 5262.

3 H. Engelkamp and S. Middelbeek, *Science*, 1999, **284**, 785.

4 (a) T. Kato, *Science*, 2002, **295**, 2414; (b) T. Scheibel, R. Parthasarathy, G. Sawicki, X. M. Lin, H. Jaeger and S. L. Lindquist, *Proc. Natl. Acad. Sci. U. S. A.*, 2003, **100**, 4527.
5 (a) S. I. Stupp, V. LeBonheur, K. Walker, L. S. Li, K. E. Huggins, M. Keser and A. Amstutz, *Science*, 1997, **276**, 384; (b) S. A. Jenekhe and X. L. Chen, *Science*, 1999, **283**, 372.
6 R. Oda, I. Huc, M. Schmutz, S. J. Candau and F. C. MacKintosh, *Nature*, 1999, **399**, 566.
7 (a) G. C. L. Wong, J. X. Tang, A. Lin, Y. L. Li, P. A. Janmey and C. R. Safinya, *Science*, 2000, **288**, 2035; (b) W. J. Blau and A. J. Fleming, *Science*, 2004, **304**, 1457.
8 (a) L. F. Zhang and A. Eisenberg, *Science*, 1995, **268**, 1728; (b) B. M. Discher, Y. Y. Won, D. S. Ege, J. C. M. Lee, F. S. Bates, D. E. Discher and D. A. Hammer, *Science*, 1999, **284**, 1143; (c) D. E. Discher and A. Eisenberg, *Science*, 2002, **297**, 967.
9 (a) J. Z. Du and R. K. O'Reilly, *Chem. Soc. Rev.*, 2011, **40**, 2402; (b) P. Broz, S. Driamov, J. Ziegler, N. Ben-Haim, S. Marsch, W. Meier and P. Hunziker, *Nano Lett.*, 2006, **6**, 2349; (c) J. D. Hartgerink, E. Beniash and S. I. Stupp, *Science*, 2001, **294**, 1684; (d) A. Rosler, G. W. M. Vandermeulen and H. A. Klok, *Adv. Drug Deliv. Rev.*, 2012, **64**, 270; (e) C. R. Safinya and K. K. Ewert, *Nature*, 2012, **489**, 372.
10 (a) S. Jain and F. S. Bates, *Science*, 2003, **300**, 460; (b) X. S. Wang, G. Guerin, H. Wang, Y. S. Wang, I. Manners and M. A. Winnik, *Science*, 2007, **317**, 644; (c) J. C. van Hest, D. A. Delnoye, M. W. Baars, M. H. van Genderen and E. W. Meijer, *Science*, 1995, **268**, 1592; (d) H. G. Cui, Z. Y. Chen, S. Zhong, K. L. Wooley and D. J. Pochan, *Science*, 2007, **317**, 647; (e) Y. Wang, H. Xu and X. Zhang, *Adv. Mater.*, 2009, **21**, 2849.
11 (a) G. Srinivas, D. E. Discher and M. L. Klein, *Nat. Mater.*, 2004, **3**, 638; (b) S. L. Lin, N. Numasawa, T. Nose and J. P. Lin, *Macromolecules*, 2007, **40**, 1684; (c) C. H. Cai, Y. L. Li, J. P. Lin, L. Q. Wang, S. L. Lin, X. S. Wang and T. Jiang, *Angew. Chem., Int. Ed.*, 2013, **52**, 7732; (d) Y. Y. Han, H. Z. Yu, H. B. Du and W. Jiang, *J. Am. Chem. Soc.*, 2009, **132**, 1144.
12 R. D. Groot and P. B. Warren, *J. Chem. Phys.*, 1997, **107**, 4423.
13 (a) Z. L. Li and E. E. Dormidontova, *Macromolecules*, 2010, **43**, 3521; (b) Z. L. Li and E. E. Dormidontova, *Soft Matter*, 2011, **7**, 4179.
14 (a) A. Nikoubashman, R. A. Register and A. Z. Panagiotopoulos, *Soft Matter*, 2013, **9**, 9960; (b) A. Nikoubashman, R. A. Register and A. Z. Panagiotopoulos, *Macromolecules*, 2013, **46**, 6651; (c) A. Nikoubashman, R. A. Register and A. Z. Panagiotopoulos, *Macromolecules*, 2014, **47**, 1193.
15 H. Y. Chen and E. Ruckenstein, *Langmuir*, 2013, **29**, 5428.
16 (a) H. Y. Chang, Y. L. Lin, Y. J. Sheng and H. K. Tsao, *Macromolecules*, 2012, **45**, 4778; (b) Y. L. Lin, H. Y. Chang, Y. J. Sheng and H. K. Tsao, *Macromolecules*, 2012, **45**, 7143; (c) H. Y. Chang, Y. L. Lin, Y. J. Sheng and H. K. Tsao, *Macromolecules*, 2013, **46**, 5644; (d) Y. L. Lin, H. Y. Chang, Y. J. Sheng and H. K. Tsao, *Soft Matter*, 2014, **10**, 1840; (e) H. Y. Chang, Y. J. Sheng and H. K. Tsao, *Soft Matter*, 2014, **10**, 6373.
17 (a) X. J. Li, I. V. Pivkin, H. J. Liang and G. E. Karniadakis, *Macromolecules*, 2009, **42**, 3195; (b) X. J. Li, Y. H. Tang, H. J. Liang and G. E. Karniadakis, *Chem. Commun.*, 2014, **50**, 8306.
18 (a) H. J. Qian, Z. Y. Lu, L. J. Chen, Z. S. Li and C. C. Sun, *Macromolecules*, 2005, **38**, 1395; (b) Y. T. Liu, Y. Zhao, H. Liu, Y. H. Liu and Z. Y. Lu, *J. Phys. Chem. B*, 2009, **113**, 15256; (c) Y. Zhao, L. Y. You, Z. Y. Lu and C. C. Sun, *Polymer*, 2009, **50**, 5333.
19 (a) D. A. Tomalia and J. M. J. Frechet, *J. Polym. Sci. Pol. Chem.*, 2002, **40**, 2719; (b) C. Gao and D. Y. Yan, *Prog. Polym. Sci*, 2004, **29**, 183; (c) D. Y. Yan, C. Gao and H. Frey, *Hyperbranched polymers: synthesis, properties, and applications*, John Wiley & Sons, Inc., Canada, 2011.
20 (a) B. Voit, *J. Polym. Sci. Pol. Chem.*, 2005, **43**, 2679; (b) B. I. Voit and A. Lederer, *Chem. Rev.*, 2009, **109**, 5924; (c) S. Peleshanko and V. V. Tsukruk, *Prog. Polym. Sci*, 2008, **33**, 523.
21 (a) Y. F. Zhou and D. Y. Yan, *Chem. Commun.*, 2009, 1172; (b) Y. F. Zhou, W. Huang, J. Y. Liu, X. Y. Zhu and D. Y. Yan, *Adv. Mater.*, 2010, **22**, 4567; (c) H. B. Jin, W. Huang, X. Y. Zhu, Y. F. Zhou and D. Y. Yan, *Chem. Soc. Rev.*, 2012, **41**, 5986.
22 (a) Y. L. Wang, B. Li, Y. F. Zhou, Z. Y. Lu and D. Y. Yan, *Soft Matter*, 2013, **9**, 3293; (b) Y. L. Wang, B. Li, H. B. Jin, Y. F. Zhou, Z. Y. Lu and D. Y. Yan, *Chem. Asian J.*, 2014, **9**, 2281.
23 (a) Y. Y. Mai, Y. F. Zhou, D. Y. Yan and H. W. Lu, *Macromolecules*, 2003, **36**, 9667; (b) B. Voit, *J. Polym. Sci. Part A: Polym. Chem.*, 2000, **38**, 2505.
24 X. Y. Zhu, Y. F. Zhou and D. Y. Yan, *J. Polym. Sci., Part B Polym. Phys.*, 2011, **49**, 1277.
25 H. X. Cheng, X. J. Yuan, X. Y. Sun, K. P. Li, Y. F. Zhou and D. Y. Yan, *Macromolecules*, 2010, **43**, 1143.
26 P. J. Hoogerbrugge and J. M. V. A. Koelman, *Europhys. Lett.*, 1992, **19**, 155.
27 P. Espanol and P. Warren, *Europhys. Lett.*, 1995, **30**, 191.
28 (a) D. Holter, A. Burgath and H. Frey, *Acta Polym.*, 1997, **48**, 30. (b) D. Holter and H. Frey, *Acta Polym.*, 1997, **48**, 298.
29 R. D. Groot and K. L. Rabone, *Biophys. J.*, 2001, **81**, 725.
30 Y. Liu, C. Y. Yu, H. B. Jin, B. B. Jiang, X. Y. Zhu, Y. F. Zhou, Z. Y. Lu and D. Y. Yan, *J. Am. Chem. Soc.*, 2013, **135**, 4765.
31 (a) Y. S. Xia, T. D. Nguyen, M. Yang, B. D. Lee, A. Santos, P. Podsiadlo, Z. Y. Tang, S. C. Glotzer and N. A. Kotov, *Nat. Nanotech.*, 2011, **6**, 580; (b) J. A. Anderson, C. D. Lorenz and A. Travesset, *J. Comput. Phys.*, 2008, **227**, 5342; (c) C. L. Phillips, J. A. Anderson and S. C. Glotzer, *J. Comput. Phys.* 2011, **230**, 7191.
32 M. Rubinstein and R. H. Colby, *Polymer Physics*, Oxford Univ Press, Oxford, 2003.
33 (a) J. Rudnick and G. Gaspari, *J. Phys. A: Math. Gen.*, 1986, **19**, 191; (b) C. M. Lin, Y. Z. Chen, Y. J. Sheng and H. K. Tsao, *React. & Funct. Polym.*, 2009, **69**, 539; (c) B. Li, L. Zhao, H. J. Qian and Z. Y. Lu, *Soft Matter*, 2014, **10**, 2245.
34 (a) H. Noguchi and K. Yoshikawa, *J. Chem. Phys.*, 1998, **109**, 5070; (b) T. Zhou and S. B. Chen, *Macromolecules*, 2005, **38**, 8554.
35 A. Patti, *Colloid Surf. A: Physicochem. Eng. Asp.*, 2010, **361**, 81.
36 J. X. Zhang, X. D. Li and X. H. Li, *Prog. Polym. Sci.*, 2012, **37**, 1130.
37 H. X. Cheng, S. G. Wang, J. T. Yang, Y. F. Zhou and D. Y. Yan, *J. Colloid Interface Sci.*, 2009, **337**, 278.
38 A. Carlmark, C. J. Hawker, A. Hult and M. Malkoch, *Chem. Soc. Rev.*, 2009, **38**, 352.

Dissipative Particle Dynamics Simulation Study on Self-Assembly of Amphiphilic Hyperbranched Multiarm Copolymers with Different Degrees of Branching

Haina Tan,[a] Wei Wang,[b] Chunyang Yu,*[a] Yongfeng Zhou,*[a] Zhongyuan Lu*[b] and Deyue Yan[a]

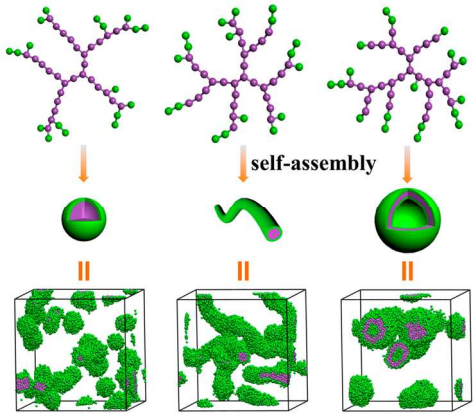

This work demonstrates the effect of degrees of branching on the self-assembly of amphiphilic hyperbranched polymers by dissipative particle dynamics simulations.